Research Article | Vol. 25, No. 9 | 1 May 2017 | OPTICS EXPRESS 9872

Optics EXPRESS

Vector optical coherence lattices generating controllable far-field beam profiles

CHUNHAO LIANG,[1,2] CHENKUN MI,[1,2] FEI WANG,[1,2] CHENGLIANG ZHAO,[1,2,4] YANGJIAN CAI,[1,2,5] AND SERGEY A. PONOMARENKO[3,6]

[1]*College of Physics, Optoelectronics and Energy & Collaborative Innovation Center of Suzhou Nano Science and Technology, Soochow University, Suzhou 215006, China*
[2]*Key Lab of Advanced Optical Manufacturing Technologies of Jiangsu Province & Key Lab of Modern Optical Technologies of Education Ministry of China, Soochow University, Suzhou 215006, China*
[3]*Department of Electrical and Computer Engineering, Dalhousie University, Halifax, Nova Scotia B3J2X4, Canada*
[4]*zhaochengliang@suda.edu.cn*
[5]*yangjiancai@suda.edu.cn*
[6]*serpo@dal.ca*

Abstract: We introduce partially coherent vector sources with periodic spatial coherence properties, which we term vector optical coherence lattices (VOCLs), as an extension of recently introduced scalar OCLs. We derive the realizability conditions and propagation formulae for radially polarized VOCLs (i.e., a typical kind of VOCLs). We show that radially polarized VOCLs display nontrivial propagation properties and generate controllable intensity lattices in the far zone of the source (or in the focal plane of a lens). By adjusting source coherence, one can obtain intensity lattices with bright or dark nodes. The latter can be employed to simultaneously trap multiple particles or atoms as well as in free-space optical communications. We also report the experimental generation of radially polarized VOCLs and we characterize VOCLs propagation properties.

OCIS codes: (030.0030) Coherence and statistical optics; (260.5430) Polarization; (140.3300) Laser beam shaping.

References and links

1. P. Senthilkumaran and R. S. Sirohi, "Michelson interferometers in tandem for array generation," Opt. Commun. **105**(3–4), 158–160 (1994).
2. S. Vyas and P. Senthilkumaran, "Interferometric optical vortex array generator," Appl. Opt. **46**(15), 2893–2898 (2007).
3. M. Kumar and J. Joseph, "Optical generation of a spatially variant two-dimensional lattice structure by using a phase only spatial light modulator," Appl. Phys. Lett. **105**(5), 051102 (2014).
4. P. Kurzynowski, W. A. Wozniak, and M. Borwinska, "Regular lattices of polarization singularities: their generation and properties," J. Opt. **12**(3), 035406 (2010).
5. M. Sakamoto, K. Oka, R. Morita, and N. Murakami, "Stable and flexible ring-shaped optical-lattice generation by use of axially symmetric polarization elements," Opt. Lett. **38**(18), 3661–3664 (2013).
6. L. Zhu, J. Yu, D. Zhang, M. Sun, and J. Chen, "Multifocal spot array generated by fractional Talbot effect phase-only modulation," Opt. Express **22**(8), 9798–9808 (2014).
7. D. Jaksch, C. Bruder, J. I. Cirac, C. W. Gardiner, and P. Zoller, "Cold bosonic atoms in optical lattices," Phys. Rev. Lett. **81**(15), 3108–3111 (1998).
8. I. Bloch, "Ultracold quantum gases in optical lattices," Nat. Phys. **1**(1), 23–30 (2005).
9. M. Takamoto, F. L. Hong, R. Higashi, and H. Katori, "An optical lattice clock," Nature **435**(7040), 321–324 (2005).
10. M. P. MacDonald, G. C. Spalding, and K. Dholakia, "Microfluidic sorting in an optical lattice," Nature **426**(6965), 421–424 (2003).
11. E. Betzig, "Excitation strategies for optical lattice microscopy," Opt. Express **13**(8), 3021–3036 (2005).
12. E. Ostrovskaya and Y. Kivshar, "Photonic crystals for matter waves: Bose-Einstein condensates in optical lattices," Opt. Express **12**(1), 19–29 (2004).
13. N. Guérineau, B. Harchaoui, J. Primot, and K. Heggarty, "Generation of achromatic and propagation-invariant spot arrays by use of continuously self-imaging gratings," Opt. Lett. **26**(7), 411–413 (2001).
14. L. Ma and S. A. Ponomarenko, "Optical coherence gratings and lattices," Opt. Lett. **39**(23), 6656–6659 (2014).
15. L. Ma and S. A. Ponomarenko, "Free-space propagation of optical coherence lattices and periodicity reciprocity," Opt. Express **23**(2), 1848–1856 (2015).

#290900 https://doi.org/10.1364/OE.25.009872
Journal © 2017 Received 17 Mar 2017; revised 16 Apr 2017; accepted 17 Apr 2017; published 19 Apr 2017

Optics EXPRESS

16. X. Liu, J. Yu, Y. Cai, and S. A. Ponomarenko, "Propagation of optical coherence lattices in the turbulent atmosphere," Opt. Lett. **41**(18), 4182–4185 (2016).
17. Y. Chen, S. A. Ponomarenko, and Y. Cai, "Experimental generation of optical coherence lattices," Appl. Phys. Lett. **109**(6), 061107 (2016).
18. Q. Zhan, "Cylindrical vector beams: from mathematical concepts to applications," Adv. Opt. Photonics **1**(1), 1–57 (2009).
19. K. Youngworth and T. Brown, "Focusing of high numerical aperture cylindrical-vector beams," Opt. Express **7**(2), 77–87 (2000).
20. D. Biss and T. Brown, "Cylindrical vector beam focusing through a dielectric interface," Opt. Express **9**(10), 490–497 (2001).
21. G. Wu, F. Wang, and Y. Cai, "Generation and self-healing of a radially polarized Bessel-Gaussian beam," Phys. Rev. A **89**(4), 043807 (2014).
22. F. Gori, "Matrix treatment for partially polarized, partially coherent beams," Opt. Lett. **23**(4), 241–243 (1998).
23. E. Wolf, *Introduction to the Theory of Coherence and Polarization of Light* (Cambridge University, 2007).
24. E. Wolf, "Unified theory of coherence and polarization of random electromagnetic beams," Phys. Lett. A **312**(5–6), 263–267 (2003).
25. F. Gori, V. Ramírez-Sánchez, M. Santarsiero, and T. Shirai, "On genuine cross-spectral density matrices," J. Opt. A, Pure Appl. Opt. **11**(8), 085706 (2009).
26. J. Tervo, T. Setälä, and A. Friberg, "Degree of coherence for electromagnetic fields," Opt. Express **11**(10), 1137–1143 (2003).
27. F. Gori, M. Santarsiero, G. Piquero, R. Borghi, A. Mondello, and R. Simon, "Partially polarized Gaussian Schell-model beams," J. Opt. A, Pure Appl. Opt. **3**(1), 1–9 (2001).
28. O. Korotkova, M. Salem, and E. Wolf, "Beam conditions for radiation generated by an electromagnetic Gaussian Schell-model source," Opt. Lett. **29**(11), 1173–1175 (2004).
29. Y. Cai, F. Wang, C. Zhao, S. Zhu, G. Wu, and Y. Dong, "Partially coherent vector beams: from theory to experiment," in *Vectorial Optical Fields: Fundamentals and Applications*, Q. Zhan, ed. (World Scientific, 2013), Chap. 7, pp. 221–273.
30. Y. Cai, Y. Chen, J. Yu, X. Liu, and L. Liu, "Generation of partially coherent beams," Prog. Opt. **62**, 157–223 (2017).
31. Y. Dong, Y. Cai, C. Zhao, and M. Yao, "Statistics properties of a cylindrical vector partially coherent beam," Opt. Express **19**(7), 5979–5992 (2011).
32. F. Wang, Y. Cai, Y. Dong, and O. Korotkova, "Experimental generation of a radially polarized beam with controllable spatial coherence," Appl. Phys. Lett. **100**(5), 051108 (2012).
33. Y. Chen, F. Wang, L. Liu, C. Zhao, Y. Cai, and O. Korotkova, "Generation and propagation of a partially coherent vector beam with special correlation functions," Phys. Rev. A **89**(1), 013801 (2014).
34. Y. Dong, F. Wang, C. Zhao, and Y. Cai, "Effect of spatial coherence on propagation, tight focusing and radiation forces of an azimuthally polarized beam," Phys. Rev. A **86**(1), 013840 (2012).
35. D. P. Brown and T. G. Brown, "Partially correlated azimuthal vortex illumination: coherence and correlation measurements and effects in imaging," Opt. Express **16**(25), 20418–20426 (2008).
36. O. Korotkova and E. Wolf, "Changes in the state of polarization of a random electromagnetic beam on propagation," Opt. Commun. **246**(1–3), 35–43 (2005).
37. H. Roychowdhury, S. A. Ponomarenko, and E. Wolf, "Changes in polarization of partially coherent electromagnetic beams propagating through the turbulent atmosphere," J. Mod. Opt. **52**(11), 1611–1618 (2005).
38. O. Korotkova, M. Salem, A. Dogariu, and E. Wolf, "Changes in the polarization ellipse of random electromagnetic beams propagating through the turbulent atmosphere," Waves Random Complex Media **15**(3), 353–364 (2005).
39. Y. Cai, O. Korotkova, H. T. Eyyuboğlu, and Y. Baykal, "Active laser radar systems with stochastic electromagnetic beams in turbulent atmosphere," Opt. Express **16**(20), 15834–15846 (2008).
40. S. Sahin, Z. Tong, and O. Korotkova, "Sensing of semi-rough targets embedded in atmospheric turbulence by means of stochastic electromagnetic beams," Opt. Commun. **283**(22), 4512–4518 (2010).
41. F. Wang, X. Liu, L. Liu, Y. Yuan, and Y. Cai, "Experimental study of the scintillation index of a radially polarized beam with controllable spatial coherence," Appl. Phys. Lett. **103**(9), 091102 (2013).
42. Y. Zhang, B. Ding, and T. Suyama, "Trapping two types of particles using a double-ring-shaped radially polarized beam," Phys. Rev. A **81**(2), 023831 (2010).
43. D. P. Brown and T. G. Brown, "Coherence measurements applied to critical and Köhler vortex illumination," Proc. SPIE **7184**, 71840B (2009).
44. Q. Lin and Y. Cai, "Tensor ABCD law for partially coherent twisted anisotropic Gaussian-Schell model beams," Opt. Lett. **27**(4), 216–218 (2002).

1. Introduction

Optical lattices with periodic intensity, polarization and phase patterns have been examined theoretically and generated experimentally [1–6]. They have also found numerous applications to atom cooling and trapping [7], ultracold quantum gas trapping [8], atomic clocks [9], microfluidic sorting [10], lattice light-sheet microscopy [11] and photonic crystal

Optics EXPRESS

engineering [12]. Besides the methods mentioned in [1–6], one can also generate intensity lattices through Tablot imaging of optical gratings because the optical gratings display transverse periodic properties [13]. The above mentioned optical lattices are generated by coherent light fields. Recently, a new kind of optical lattices named optical coherence lattices (OCLs) was introduced in [14, 15], where the OCLs are generated by partially coherent light sources with periodic coherence properties. It was shown in [14, 15] that the OCLs exhibit periodicity reciprocity: the initial periodic degree of coherence transfers its periodicity to the periodic intensity distribution on propagation in free-space. In other words, the OCLs yield intensity lattices with bright nodes in the far field (or in the focal plane of an imaging lens). This property, unique to partially coherent sources, is useful for simultaneously trapping multiple particles whose refractive indices are larger than that of the ambient. In the turbulent atmosphere, it was shown [16] that the OCLs also display the periodicity reciprocity over long propagation distances and they have scintillation indices lower than those of Gaussian beams, even though the lattices are eventually affected by the turbulence. The discovered periodicity reciprocity makes OCLs attractive for robust free-space optical communications [14–16]. More recently, experimental generation of OCLs was reported and it was shown that the OCLs may find applications to image transmission and optical encryption [17]. However, all research on OCLs has so far focused on scalar light fields.

At the same time, polarization is a fundamental property of light fields. Depending on its polarization state, electromagnetic beams can be classified as uniformly polarized vector beams and non-uniformly polarized vector beams. Cylindrical vector beams, such as radially polarized and azimuthally polarized beams, are typical kinds of non-uniformly polarized vector beams [18]. Due to their tight focusing properties [19, 20] and self-healing potential [21], cylindrical vector beams have found applications to optical trapping, microscopy, optical data storage, lithography, proton acceleration, electron acceleration, material processing, plasmonic focusing, dark imaging, high-resolution metrology, free-space optical communication, super-resolution imaging and laser machining [18], among other venues. Partially coherent vector beams can be described in terms of their beam coherence-polarization (BCP) matrices in the space-time representation [22] or their cross-spectral density matrices in the space-frequency representation [23]. A unified theory of coherence and polarization for partially coherent vector beams was developed by Wolf in 2003 [24], and the conditions for devising bona fide cross-spectral density matrices were introduced by Gori et al. in 2009 [25]. Different definitions of the degree of coherence of partially coherent vector beams were developed [24, 26]. Partially coherent vector beams with either uniform or non-uniform states of polarization (SOP) were explored theoretically and generated experimentally [27–35]. One of the key properties of a partially coherent vector beam SOP is its ability to change on propagation in free space [36]. Further, the degree of polarization was shown to regain its magnitude at the source over sufficiently long distance in the turbulent atmosphere [37, 38], making such beams attractive for free-space optical communications, laser radar system and remote sensing [39–41]. By adjusting the coherence width of a non-uniformly polarized partially coherent vector beam, we can generate a Gaussian-like beam spot or a flat-topped beam spot or a dark hollow beam spot in the far field [32–34], which can come in handy for material thermal processing and for trapping a Rayleigh particle whose refractive index is larger or smaller than that of the ambient [34, 42]. In [35, 43], a class of partially coherent vector beams, partially correlated azimuthal vortices, were employed in illuminating an imaging system. It was discovered that the image contrast can be thereby improved, which carries potential for metrology, microscopy, and lithography.

The coherence properties of previously studied vector beams display no periodicity at the source. In this work, we propose partially coherent vector beams with periodic spatial coherence properties, vector optical coherence lattices (VOCLs) as a natural extension of recently introduced scalar optical coherence lattices. The most interesting property of VOCLs is that the initial single radially polarized beam spot evolves into multiple radially polarized

Optics EXPRESS

beam spots with bright or dark beam profiles in the far zone of the source (or in the focal plane of a lens), in other words, the VOCLs generate intensity lattices with bright or dark nodes depending on the magnitude of a controlled source coherence parameter. The scalar OCLs in our previous papers can only generate intensity lattices with bright nodes [14–17]. The introduced VOCLs are expected to be useful for simultaneous trapping of multiple particles or atoms and for free-space optical communications.

2. Theoretical models for vector optical coherence lattices and realizability conditions

In this section, we will introduce a theoretical model for VOCLs and discuss their realizability conditions. The degree of coherence of scalar OCLs can be expressed as [14, 17]

$$\mu(\mathbf{r}_1,\mathbf{r}_2)=\frac{2}{M}\sum_{m=1}^{M}\frac{\mathrm{J}_1\left(|\mathbf{r}_1-\mathbf{r}_2|/\sqrt{2}\delta\right)}{|\mathbf{r}_1-\mathbf{r}_2|/\sqrt{2}\delta}\exp\left[i\mathbf{V}_{0m}\cdot(\mathbf{r}_1-\mathbf{r}_2)\right]. \tag{1}$$

Here δ and $\mathbf{V}_{0m}$ are coherence and phase parameters, respectively. One can synthetize scalar OCLs through, for instance, a superposition of multiple Schell-model beams with prescribed degrees of coherence [17].

Consider a 2×2 BCP matrix $\hat{\Gamma}(\mathbf{r}_1,\mathbf{r}_2)$ of the source, defined as [22]

$$\Gamma_{\alpha\beta}(\mathbf{r}_1,\mathbf{r}_2)=\left\langle E_\alpha^*(\mathbf{r}_1)E_\beta(\mathbf{r}_2)\right\rangle,\ (\alpha,\beta=x,y). \tag{2}$$

Here the angle brackets denote ensemble averaging and $\mathbf{r}_1\equiv(x_1,y_1)$ and $\mathbf{r}_2\equiv(x_2,y_2)$ are transverse position vectors in the source plane; $E_\alpha(\mathbf{r})$ is a fluctuating electric field component along the α axis at point $\mathbf{r}$.

To be a bona fide BCP matrix, the elements of the BCP matrix can be expressed as [25]

$$\Gamma_{\alpha\beta}(\mathbf{r}_1,\mathbf{r}_2)=\int P_{\alpha\beta}(\mathbf{v})H_\alpha(\mathbf{r}_1,\mathbf{v})H_\beta^*(\mathbf{r}_2,\mathbf{v})\,\mathrm{d}^2\mathbf{v}, \tag{3}$$

where $\mathbf{v}\equiv(v_x,v_y)$, H_α is an arbitrary kernel, $P_{\alpha\beta}(\mathbf{v})$ are the elements of the 2×2 non-negative definite matrix $\hat{P}$ that satisfy the following constraints

$$P_{\alpha\alpha}(\mathbf{v})\ge0,\quad P_{xx}(\mathbf{v})P_{yy}(\mathbf{v})-\left|P_{xy}(\mathbf{v})\right|^2\ge0. \tag{4}$$

To obtain VOCLs, we define H_α and $P_{\alpha\beta}$ as follows

$$H_\alpha(\mathbf{r},\mathbf{v})=-\frac{i}{\lambda f}T_\alpha\exp\left[\frac{i\pi}{\lambda f}\left(\mathbf{v}^2-2\mathbf{r}\cdot\mathbf{v}\right)\right], \tag{5}$$

$$P_{\alpha\beta}(\mathbf{v})=\frac{B_{\alpha\beta}}{MN}\sum_{m=-(M-1)/2}^{(M-1)/2}\sum_{n=-(N-1)/2}^{(N-1)/2}\mathrm{circ}\left(\frac{\mathbf{v}-\mathbf{v}_{mn}}{a_{\alpha\beta}}\right). \tag{6}$$

Here H_α can be regarded as a transfer function of an optical path consisting of free space of distance f, a thin lens with the focal length f and a spatial filter with a transmission function T_α. Further, λ is the wavelength of the light field. $P_{\alpha\beta}(\mathbf{v})$ can be regarded as a superposition of multiple circ functions with a radius $a_{\alpha\beta}$ and off-axis displacements $\mathbf{v}_{mn}=(md,nd)$; d denotes the separation between adjacent circ functions, M and N stand for the numbers of the

Optics EXPRESS

circ functions along x and y directions, respectively. $B_{\alpha\beta}=\left|B_{\alpha\beta}\right|\exp\left(i\phi_{\alpha\beta}\right)$ are the correlation coefficients between the field components E_α and E_β.

Substituting from Eqs. (5) and (6) into Eq. (3), we obtain the elements of the BCP matrix of VOCLs as

$$\Gamma_{\alpha\beta}\left(\mathbf{r}_1,\mathbf{r}_2\right)=C_0T_\alpha^*T_\beta\gamma_{\alpha\beta}\left(\mathbf{r}_1,\mathbf{r}_2\right), \tag{7}$$

where C_0 is a constant, $\gamma_{\alpha\beta}\left(\mathbf{r}_1,\mathbf{r}_2\right)$ represent the correlation functions given by

$$\gamma_{\alpha\beta}\left(\mathbf{r}_1,\mathbf{r}_2\right)=\frac{2B_{\alpha\beta}}{MN}\sum_{m=-(M-1)/2}^{(M-1)/2}\sum_{n=-(N-1)/2}^{(N-1)/2}\frac{J_1\left(\left|\mathbf{r}_1-\mathbf{r}_2\right|/\sqrt{2}\delta_{0\alpha\beta}\right)}{\left|\mathbf{r}_1-\mathbf{r}_2\right|/\sqrt{2}\delta_{0\alpha\beta}}\exp\left[-\frac{i2\pi}{\lambda f}\mathbf{v}_{mn}\cdot\left(\mathbf{r}_1-\mathbf{r}_2\right)\right]. \tag{8}$$

Here $\delta_{0\alpha\beta}=f/\sqrt{2}ka_{\alpha\beta}$ are referred to as coherence parameters. Comparing Eqs. (1) and (8), we infer that the expressions of the correlation functions of VOCLs are similar to the expression of the degree of coherence of scalar OCLs.

The VOCL SOP is closely related to T_α. If we set $T_\alpha=A_\alpha\exp\left(-\frac{\mathbf{r}^2}{4w_s^2}\right),(\alpha=x,y)$ with A_α and w_s being a constant and the beam width, respectively, VOCLs exhibit uniform SOP (i.e., the state of polarization of any point in the source plane is the same) and are called uniformly polarized VOCLs. If we set $T_\alpha=\frac{\alpha}{2w_s^2}\exp\left(-\frac{\mathbf{r}^2}{4w_s^2}\right),(\alpha=x,y)$ or $T_x=\frac{y}{2w_s^2}\exp\left(-\frac{\mathbf{r}^2}{4w_s^2}\right)$ and $T_y=\frac{x}{2w_s^2}\exp\left(-\frac{\mathbf{r}^2}{4w_s^2}\right)$, VOCLs exhibit non-uniform SOP (radial or azimuthal polarization) and are termed radially or azimuthally polarized VOCLs.

Hereafter, we mainly focus on radially polarized VOCLs, which can be readily generated in the laboratory. First, we discuss the realizability conditions. To be a physically realizable partially coherent vector beam, it is known that the BCP matrix of VOCLs should be quasi-Hermitian [25], namely $\Gamma_{\alpha\beta}\left(\mathbf{r}_1,\mathbf{r}_2\right)=\Gamma_{\beta\alpha}^*\left(\mathbf{r}_2,\mathbf{r}_1\right)$. To meet this requirement, the following conditions should be satisfied

$$\left|B_{\alpha\beta}\right|=1,\phi_{\alpha\beta}=0,(\alpha=\beta),\left|B_{\alpha\beta}\right|\le 1,(\alpha\ne\beta),\left|B_{xy}\right|=\left|B_{yx}\right|,\phi_{xy}=\phi_{yx},\delta_{0xy}=\delta_{0yx}. \tag{9}$$

To check the non-negativity conditions, substituting from Eq. (6) into Eq. (4), we obtain the following inequality

$$\sum_{m=-(M-1)/2}^{(M-1)/2}\sum_{n=-(N-1)/2}^{(N-1)/2}\mathrm{circ}\left(\frac{\mathbf{v}-\mathbf{v}_{mn}}{a_{xx}}\right)\sum_{m=-(M-1)/2}^{(M-1)/2}\sum_{n=-(N-1)/2}^{(N-1)/2}\mathrm{circ}\left(\frac{\mathbf{v}-\mathbf{v}_{mn}}{a_{yy}}\right)\ge\left|B_{xy}\right|^2\left|\sum_{m=-(M-1)/2}^{(M-1)/2}\sum_{n=-(N-1)/2}^{(N-1)/2}\mathrm{circ}\left(\frac{\mathbf{v}-\mathbf{v}_{mn}}{a_{xy}}\right)\right|^2. \tag{10}$$

Applying the equation $\mathrm{circ}\left(\mathbf{r}/a\right)\times\mathrm{circ}\left(\mathbf{r}/b\right)=\mathrm{circ}\left(\mathbf{r}/\min\left(a,b\right)\right)$, it is not difficult to derive the following inequality from Eq. (10)

$$a_{xy}\le\min\left(a_{xx},a_{yy}\right). \tag{11}$$

Equation (11) is equivalent to the following inequality

$$\delta_{0xy}\ge\max\left(\delta_{0xx},\delta_{0yy}\right). \tag{12}$$

Optics EXPRESS

To realize radially polarized VOCLs, two additional conditions should be imposed: (a) any point in the source plane is linearly polarized, (b) the orientation angle of the polarization at any point in the source plane should satisfy $\theta(x,y)=\arctan(y/x)$. It is known that the BCP matrix of a partially coherent vector beam can be represented as a sum of the BCP matrix of a completely polarized beam and the BCP matrix of a completely unpolarized beam [23, 36]. The SOP of the completely polarized beam can be characterized by the polarization ellipse, with the major and minor semi-axes of the polarization ellipse $A_1(\mathbf{r})$ and $A_2(\mathbf{r})$, the degree of ellipticity $\varepsilon(\mathbf{r})$ and the orientation angle $\theta(\mathbf{r})$ related with the elements of the BCP matrix as [23, 36]

$$A_{1,2}(\mathbf{r})=\frac{1}{\sqrt{2}}\left[\sqrt{\left(\Gamma_{xx}(\mathbf{r},\mathbf{r})-\Gamma_{yy}(\mathbf{r},\mathbf{r})\right)^2+4\left|\Gamma_{xy}(\mathbf{r},\mathbf{r})\right|^2}\pm\sqrt{\left(\Gamma_{xx}(\mathbf{r},\mathbf{r})-\Gamma_{yy}(\mathbf{r},\mathbf{r})\right)^2+4\mathrm{Re}\left|\Gamma_{xy}(\mathbf{r},\mathbf{r})\right|^2}\right]^{1/2}, \quad (13)$$

$$\varepsilon(\mathbf{r})=A_2(\mathbf{r})/A_1(\mathbf{r}), \quad (14)$$

$$\theta(\mathbf{r})=\frac{1}{2}\arctan\left[\frac{2\,\mathrm{Re}\left[\Gamma_{xy}(\mathbf{r},\mathbf{r})\right]}{\Gamma_{xx}(\mathbf{r},\mathbf{r})-\Gamma_{yy}(\mathbf{r},\mathbf{r})}\right]. \quad (15)$$

To satisfy the additional conditions (a) and (b), substituting the elements of the BCP matrix of radially polarized VOCLs into Eqs. (13)-(15), we obtain the equalities

$$B_{xy}=B_{yx}=1,\ \delta_{0xx}=\delta_{0yy}=\delta_{0xy}=\delta_{0yx}=\delta_0. \quad (16)$$

Equations (9), (12) and (16) are the realizability conditions for radially polarized VOCLs.

In this work, we set $A_x=A_y=1$. By applying Eq. (16), we find the correlation functions of the radially polarized VOCLs satisfy the following equalities

$$\gamma_{xx}(\mathbf{r}_1,\mathbf{r}_2)=\gamma_{yy}(\mathbf{r}_1,\mathbf{r}_2)=\gamma_{xy}(\mathbf{r}_1,\mathbf{r}_2)=\gamma_{yx}(\mathbf{r}_1,\mathbf{r}_2). \quad (17)$$

The electromagnetic degree of coherence of radially polarized VOCLs is defined as [26]

$$\mu^2(\mathbf{r}_1,\mathbf{r}_2)=\frac{\sum_{\alpha,\beta}\left|\Gamma_{\alpha\beta}(\mathbf{r}_1,\mathbf{r}_2)\right|^2}{\sum_{\alpha,\beta}\Gamma_{\alpha\alpha}(\mathbf{r}_1,\mathbf{r}_1)\Gamma_{\beta\beta}(\mathbf{r}_2,\mathbf{r}_2)}. \quad (18)$$

Substituting from Eqs. (7) and (17) into Eq. (18), we obtain

$$\mu^2(\mathbf{r}_1,\mathbf{r}_2)=\gamma^2_{\alpha\beta}(\mathbf{r}_1,\mathbf{r}_2)\,(\alpha,\beta=x,y). \quad (19)$$

It follows from Eq. (19) that the degree of coherence of the radially polarized VOCLs and the correlation functions are the same. To save space, we only display theoretical and experimental results for the degree of coherence $\mu^2(\mathbf{r}_1,\mathbf{r}_2)$ hereafter.

Optics EXPRESS

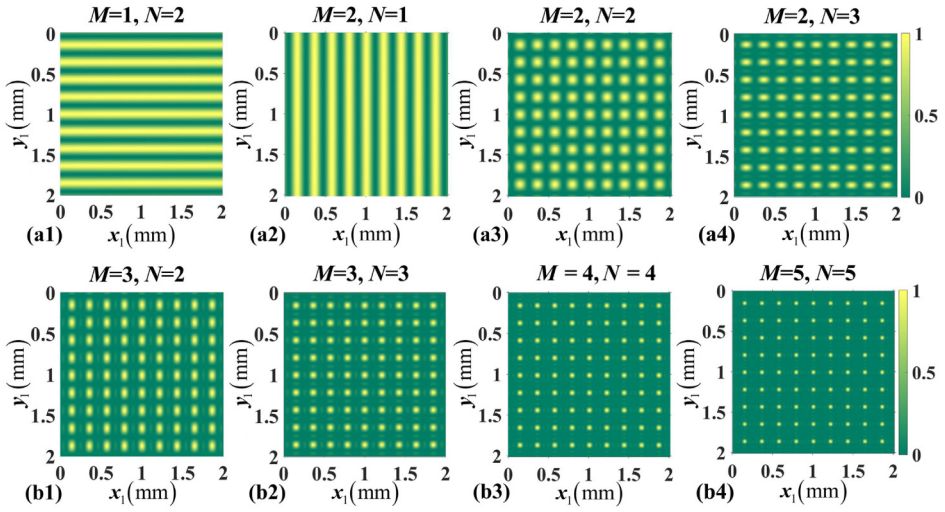

Fig. 1. Density plot of the square of the the degree of coherence $\mu^2(x_1, y_1, 1\text{mm}, 1\text{mm})$ of radially polarized VOCLs for different values of M and N with $\delta_0 = 3\text{mm}$ and $d = 1\text{mm}$ in the source plane.

Figure 1 shows the density plot of the square of the degree of coherence $\mu^2(x_1, y_1, 1\text{mm}, 1\text{mm})$ of radially polarized VOCLs for different values of M and N. We see from Fig. 1 that the degree of coherence of radially polarized VOCLs does display a lattices-like behavior when $M>1$ and $N>1$, and the lattice structure becomes more complex as the magnitudes of M and N increase.

3. Propagation properties of radially polarized vector optical coherence lattices

In this section, we will derive the analytical propagation formulae for radially polarized VOCLs and explore their propagation properties in free space numerically. The BCP matrix of a partially coherent vector beam passing through a stigmatic ABCD optical system can be expressed using the so-called generalized Collins formula as [44]

$$\Gamma_{\alpha\beta}(\boldsymbol{\rho}_1, \boldsymbol{\rho}_2) = \frac{1}{(\lambda B)^2}\exp\left[-\frac{ikD}{2B}\left(\boldsymbol{\rho}_1^2 - \boldsymbol{\rho}_2^2\right)\right]\iint \Gamma_{\alpha\beta}(\mathbf{r}_1, \mathbf{r}_2)\exp\left[-\frac{ikA}{2B}\left(\mathbf{r}_1^2 - \mathbf{r}_2^2\right)\right]\exp\left[\frac{ik}{B}\left(\mathbf{r}_1\cdot\boldsymbol{\rho}_1 - \mathbf{r}_2\cdot\boldsymbol{\rho}_2\right)\right]\mathrm{d}^2\mathbf{r}_1\mathrm{d}^2\mathbf{r}_2, \tag{20}$$

where $\boldsymbol{\rho}_1 \equiv (\rho_{1x}, \rho_{1y})$ and $\boldsymbol{\rho}_2 \equiv (\rho_{2x}, \rho_{2y})$ are transverse position vectors in the receiver plane, $k = 2\pi/\lambda$ is the wavenumber; A, B, C, and D denote optical system transfer matrix elements.

Substituting the elements of BCP matrix of radially polarized VOCLs in the source plane into Eq. (20), we obtain (after integration) the following expressions for the elements of the BCP matrix in the receiver plane

$$\Gamma_{xx}(\boldsymbol{\rho}_1, \boldsymbol{\rho}_2) = \frac{C_0\pi^2}{\lambda^2 B^2 \Delta^2 MN}\sum_{h=0}^{\infty}\sum_{s=0}^{h}\sum_{m=-(M-1)/2}^{(M-1)/2}\sum_{n=-(N-1)/2}^{(N-1)/2}\frac{(-1)^h}{2^{3h}s!(h-s)!(h+1)!\delta_0^{2h}}Q_{2s}^n(\rho_{sy}, \rho_{dy})$$
$$\times\left[-\left(\rho_{dx}^2 - \frac{B^2}{k^2 w_s^2}\right)Q_{2(h-s)}^m(\rho_{sx}, \rho_{dx}) + 2A\rho_{dx}Q_{2(h-s)+1}^m(\rho_{sx}, \rho_{dx}) - \Delta^2 Q_{2(h-s)+2}^m(\rho_{sx}, \rho_{dx})\right], \tag{21}$$

Optics EXPRESS

$$\Gamma_{yy}(\boldsymbol{\rho}_1,\boldsymbol{\rho}_2)=\frac{C_0\pi^2}{\lambda^2B^2\Delta^2MN}\sum_{h=0}^{\infty}\sum_{s=0}^{h}\sum_{m=-(M-1)/2}^{(M-1)/2}\sum_{n=-(N-1)/2}^{(N-1)/2}\frac{(-1)^h}{2^{3h}s!(h-s)!(h+1)!\delta_0^{2h}}Q^m_{2(h-s)}(\rho_{sx},\rho_{dx})$$
$$\times\left[-\left(\rho_{dy}^2-\frac{B^2}{k^2w_s^2}\right)Q^n_{2s}(\rho_{sy},\rho_{dy})+2A\rho_{dx}Q^n_{2s+1}(\rho_{sy},\rho_{dy})-\Delta^2Q^n_{2s+2}(\rho_{sy},\rho_{dy})\right], \tag{22}$$

$$\Gamma_{xy}(\boldsymbol{\rho}_1,\boldsymbol{\rho}_2)=\frac{C_0\pi^2}{\lambda^2B^2\Delta^2MN}\sum_{h=0}^{\infty}\sum_{s=0}^{h}\sum_{m=-(M-1)/2}^{(M-1)/2}\sum_{n=-(N-1)/2}^{(N-1)/2}\frac{(-1)^h}{2^{3h}s!(h-s)!(h+1)!\delta_0^{2h}} \tag{23}$$
$$\times\left[i\rho_{dx}Q^m_{2(h-s)}(\rho_{sx},\rho_{dx})-\left(iA-\frac{B}{2w_s^2k}\right)Q^m_{2(h-s)+1}(\rho_{sx},\rho_{dx})\right]\left[i\rho_{dy}Q^n_{2s}(\rho_{sy},\rho_{dy})-\left(iA+\frac{B}{2w_s^2k}\right)Q^n_{2s+1}(\rho_{sy},\rho_{dy})\right],$$

$$\Gamma_{yx}(\boldsymbol{\rho}_1,\boldsymbol{\rho}_2)=\Gamma^*_{xy}(\boldsymbol{\rho}_2,\boldsymbol{\rho}_1), \tag{24}$$

where $\boldsymbol{\rho}_s=(\boldsymbol{\rho}_1+\boldsymbol{\rho}_2)/2\equiv(\rho_{sx},\rho_{sy})$, $\boldsymbol{\rho}_d=\boldsymbol{\rho}_1-\boldsymbol{\rho}_2\equiv(\rho_{dx},\rho_{dy})$, $\Delta=\sqrt{A^2+B^2/4k^2w_s^4}$, and

$$Q^p_t(\rho_{s\alpha},\rho_{d\alpha})=\left(-\frac{iB}{\sqrt{2}kw_s\Delta}\right)^t\exp\left(-\frac{ikD}{B}\rho_{s\alpha}\rho_{d\alpha}\right)H_t\left(\frac{1}{\sqrt{2}w_s\Delta}\left(\frac{B}{f}pd-\rho_{s\alpha}+i\frac{kw_s^2A}{B}\rho_{d\alpha}\right)\right).$$
$$\times\exp\left(-\frac{k^2w_s^2}{2B^2}\rho_{d\alpha}^2\right)\exp\left(-\frac{1}{2w_s^2\Delta^2}\left(\frac{B}{f}pd-\rho_{s\alpha}+i\frac{kw_s^2A}{B}\rho_{d\alpha}\right)^2\right) \tag{25}$$

Here H_t denotes a Hermite polynomial of order t.

The average intensity of radially polarized VOCLs is obtained as [22, 23]

$$I(\boldsymbol{\rho})=\Gamma_{xx}(\boldsymbol{\rho},\boldsymbol{\rho})+\Gamma_{yy}(\boldsymbol{\rho},\boldsymbol{\rho})=I_x(\boldsymbol{\rho})+I_y(\boldsymbol{\rho}). \tag{26}$$

Applying Eqs. (13)-(15) and (21)-(26), we can study the propagation properties (e.g., average intensity and SOP) of radially polarized VOCLs in free space numerically by setting the elements of the transfer matrix of free space as $A=1, B=z, C=0, D=1$. We can study the focusing properties of radially polarized VOCLs focused by a thin lens with focal length f by setting $A=1-z/f, B=f, C=-1/f, D=0$, Here we assumed the distances from the source plane to the thin lens and from the thin lens to the receiver plane to be f and z, respectively. We note that the beam parameters in the far field and the focal plane are the same.

We now proceed to numerically study propagation properties of radially polarized VOCLs in free space. To this end, we set $w_s=0.4$mm, d=1mm and $\lambda=532.8$nm. We calculate in Figs. 2-4 the density plot of the normalized intensity distribution $I(\boldsymbol{\rho})/I_{\max}(\boldsymbol{\rho})$, the corresponding components $I_x(\boldsymbol{\rho})/I_{y\max}(\boldsymbol{\rho})$, $I_y(\boldsymbol{\rho})/I_{y\max}(\boldsymbol{\rho})$, and the radially polarized VOCLs SOP distribution at several propagation distances in free space for different values of the coherence parameter δ_0 with M = N = 3. We infer from Figs. 2-4 that the beams display instructive propagation features in free space. In particular, dark hollow beam profiles at the source gradually evolve into lattice distributions on propagation, implying that the degree of coherence transfers its periodicity to beam intensity distributions. The intensity lattices in the far field are controlled by the initial coherence parameter δ_0. Thus, we can obtain intensity lattices with dark nodes (i.e., dark hollow beam arrays) when the coherence parameter δ_0 is large (see Fig. 2), and we can obtain intensity lattices with bright nodes (i.e., flat-topped or Gaussian-like beam arrays) as we decrease the coherence parameter δ_0 (see Figs. 3 and 4). In addition, we deduce from Figs. 2-4 that the radially polarized VOCLs SOP varies on propagation, and a single radial polarized beam spot at the source evolves into multiple

Optics EXPRESS

radially polarized beam spots, which means each lattice in the far field displays radial polarization.

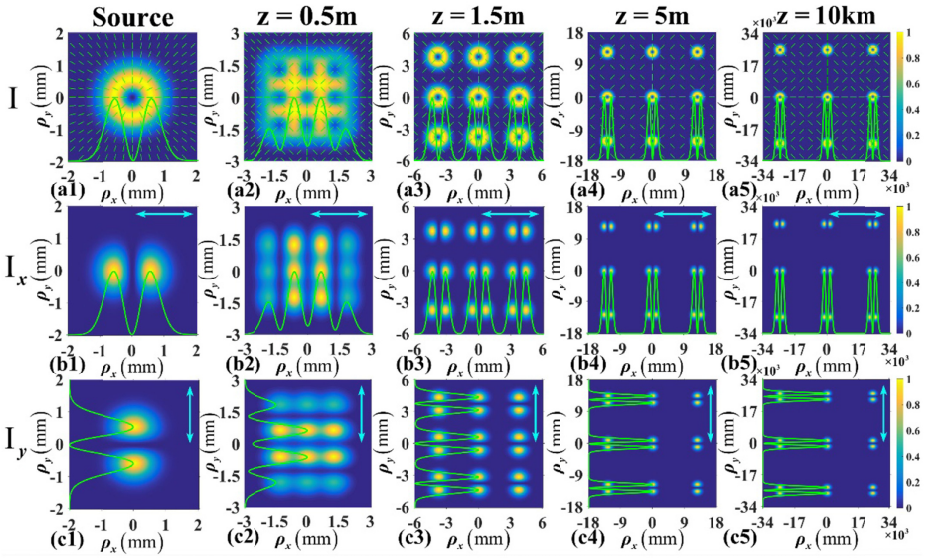

Fig. 2. Density plot of the normalized intensity distribution $I(\boldsymbol{\rho})/I_{\max}(\boldsymbol{\rho})$, the corresponding components $I_x(\boldsymbol{\rho})/I_{y\max}(\boldsymbol{\rho})$, $I_y(\boldsymbol{\rho})/I_{y\max}(\boldsymbol{\rho})$, and the distribution of the SOP of radially polarized VOCLs at several propagation distances in free space with $M = N = 3$ and $\delta_0 = 3\text{mm}$.

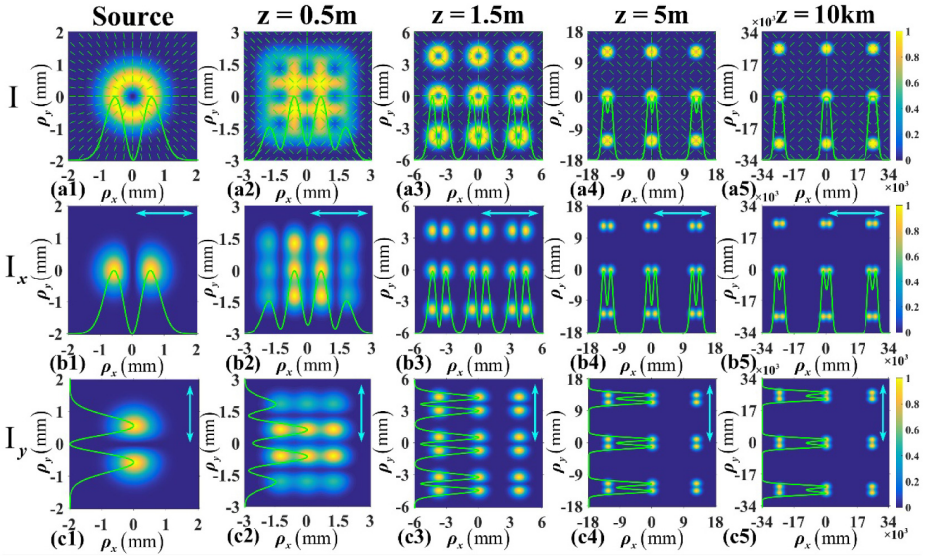

Fig. 3. Density plot of the normalized intensity distribution $I(\boldsymbol{\rho})/I_{\max}(\boldsymbol{\rho})$, the corresponding components $I_x(\boldsymbol{\rho})/I_{y\max}(\boldsymbol{\rho})$, $I_y(\boldsymbol{\rho})/I_{y\max}(\boldsymbol{\rho})$, and the distribution of the SOP of radially polarized VOCLs at several propagation distances in free space with $M = N = 3$ and $\delta_0 = 0.4\text{mm}$.

Optics EXPRESS

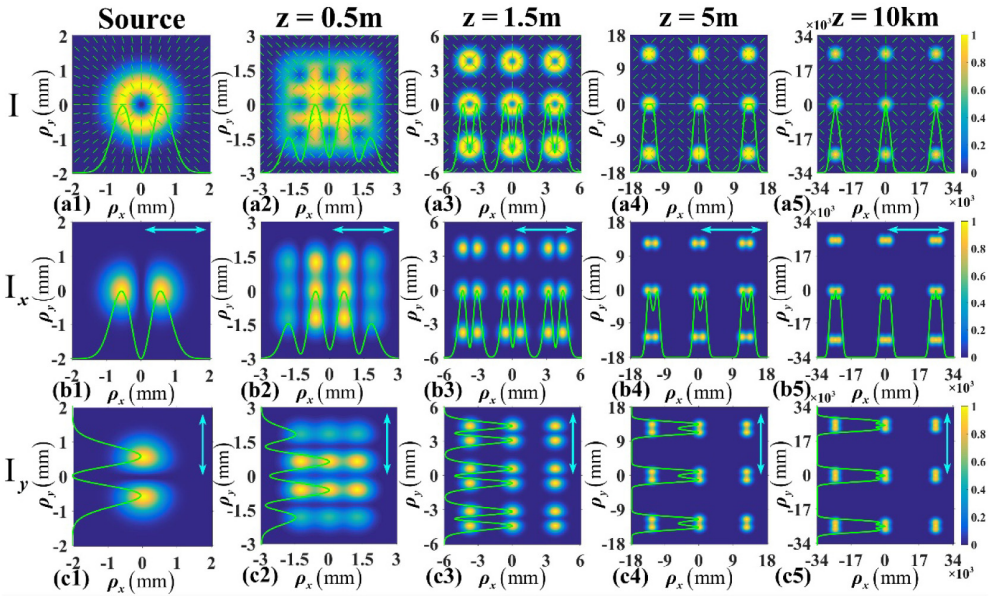

Fig. 4. Density plot of the normalized intensity distribution $I(\boldsymbol{\rho})/I_{\max}(\boldsymbol{\rho})$, the corresponding components $I_x(\boldsymbol{\rho})/I_{x\max}(\boldsymbol{\rho})$, $I_y(\boldsymbol{\rho})/I_{y\max}(\boldsymbol{\rho})$, and the distribution of the SOP of radially polarized VOCLs at several propagation distances in free space with M = N = 3 and $\delta_0 = 0.32\text{mm}$.

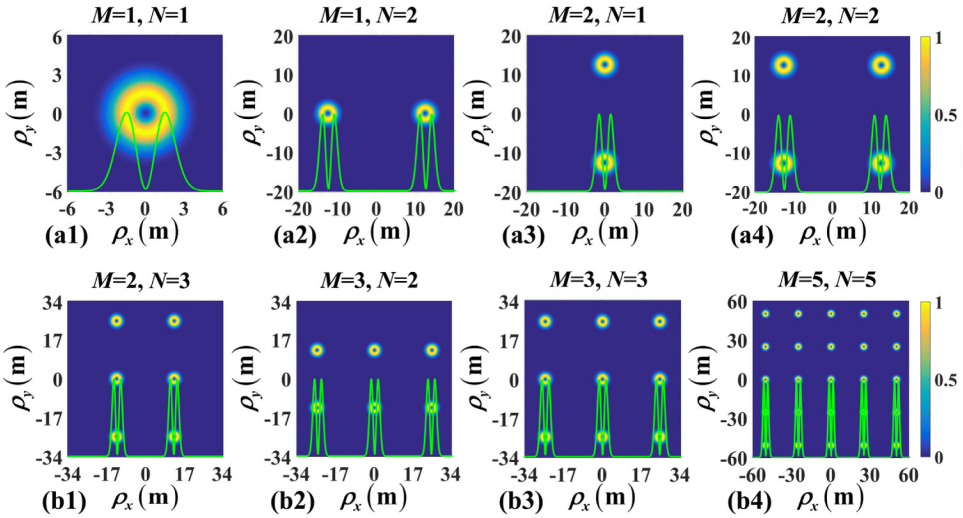

Fig. 5. Density plot of the normalized intensity distribution $I(\boldsymbol{\rho})/I_{\max}(\boldsymbol{\rho})$ of radially polarized VOCLs at $z = 10\text{km}$ in free space for different values of M and N with δ_0=3mm.

To explore the effect of the parameters M and N on the propagation properties of radially polarized VOCLs, we calculate in Fig. 5 their normalized intensity distribution $I(\boldsymbol{\rho})/I_{\max}(\boldsymbol{\rho})$ at $z = 10\text{km}$ in free space for different values of M and N with δ_0=3mm, and we find that the

Optics EXPRESS

number of dark cores equals to $M \times N$. Numerical results (not shown here) also show that the initial parameter d only affects the separation of the dark or solid cores in the far-field lattices and doesn't affect the SOP of each core. The intensity periodicity in the focal plane of a lens (or in the far zone of the source) in this work is caused by the spatial coherence periodicity in the transverse plane of the source, and this periodicity reciprocity is specific to partially coherent sources. Thus, one can modulate the distribution of the intensity lattices in the far field (or in the focal plane) conveniently through varying its initial coherence properties, which will be useful for particle trapping, e.g., the obtained intensity lattices with solid cores or dark cores in the focal plane can be used to simultaneously trap multiple particles whose refractive indices are larger or smaller than that of the ambient. The obtained intensity lattices with dark cores in the focal plane can also be utilized for simultaneous trapping of multiple atoms if the light field is blue-detuned. Furthermore, it is known that both scalar OCLs and radially polarized beams have advantage over Gaussian beams for mitigating the effect of atmospheric turbulence [16, 41]. One may expect to further mitigate the effect of atmospheric turbulence using radially polarized VOCLs, which will be useful in free-space optical communications. In our previous papers [14–17], the proposed scalar OCLs do not carry phase vortices. Thus, they generate intensity lattices with only bright nodes in the far field. In principle, one may expect to generate intensity lattices with dark nodes from scalar OLCs with phase vortices. In any case, our work clearly shows that manipulating coherence properties of a radially polarized beam provides a novel way to produce far-zone intensity lattices with bright or dark nodes.

4. Experimental generation of radially polarized vector optical coherence lattices

In this section, we report the experimental generation and characterization of radially polarized VOCLs. We employ a radial polarization converter (RPC) to convert linearly polarized VOCLs into radially polarized VOCLs. Figure 6 shows our experimental setup for generating radially polarized VOCLs and measuring its degree of coherence and focused intensity. In our experiment, a laser beam emitted by an Nd:YAG laser ($\lambda = 532\text{nm}$) first passes through a linear polarizer and a beam expander, followed by an amplitude mask (AM), which is used to modulate the intensity distribution of the incident beam. Here the AM is a $M \times N$ circular aperture array; a is the radius of each aperture and d the separation between adjacent apertures. The modulated beam from the AM illuminates a rotating ground-glass disk (RGGD), producing an incoherent beam with a prescribed intensity distribution. Here the speed of the RGGD is controlled by a motion controller. Having passed through a thin lens L_2 with the focal length $f_1 = 25\text{cm}$ and the Gaussian amplitude filter (GAF), the incoherent beam from the RGGD transforms into linearly polarized VOCLs [17]. We then convert it into a radially polarized VOCLs by the RPC. The coherence parameter of the generated beam is controlled by varying the radius of the aperture through the relation $\delta_0 = f / \sqrt{2}ka$. The experimental setup for generating linearly polarized VOCLs is the same as that reported in [17], and the key point for generating radially polarized VOCLs in our experiment is the RPC use.

Optics EXPRESS

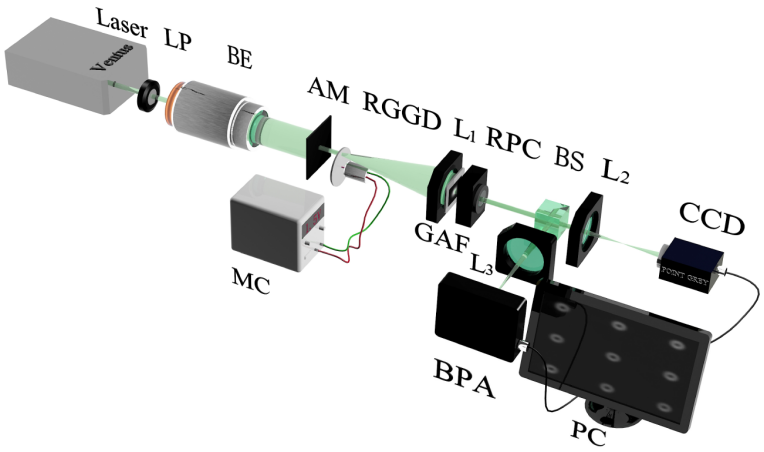

Fig. 6. Experimental setup for generating radially polarized VOCLs, measuring the degree of coherence and the focused intensity. Laser, Nd: YAG laser; LP, linear polarizer; BE, beam expander; AM, amplitude mask; L_1, L_2 and L_3, thin lenses; RGGD, rotating ground-glass disk; MC, motion controller; GAF, Gaussian amplitude filter; RPC, radial polarization converter; BS, beam splitter; CCD, charge-coupled device; BPA, beam profile analyzer; PC, personal computer.

To measure the degree of coherence and the focused intensity of the generated radially polarized VOCLs, we use a beam splitter (BS) to split the generated beam into two beams. The transmitted beam from the BS passes through the thin lens L_2 with the focal length $f_2 = 15\text{cm}$ arriving at a charge-coupled device (CCD). Both distances from RPC to L_2 and from L_2 to CCD are $2f_2$ (i.e., $2f$ imaging system) such that the VOCLs degree of coherence in the CCD plane is the same as that in the source plane (just behind the RPC). Here the CCD is used to measure the modulus of the VOCLs degree of coherence. A detailed measurement protocol can be found in [33]. The beam reflected from the BS is then transmitted through a thin lens L_3 with the focal length $f_3 = 15\text{cm}$. The resulting beam then arrives at the beam profile analyzer (BPA), which is used to measure the focused intensity distribution. The distances from the BPA to L_3 and from L_3 to BPA are f_3 and z, respectively. The elements of the transfer matrix of the optical system between the RPC and BPA are $A = 1 - z/f_3, B = f_3, C = -1/f_3, D = 0$. The components of the focused intensity I_x and I_y can be measured by adding a linear polarizer between L_3 and BPA.

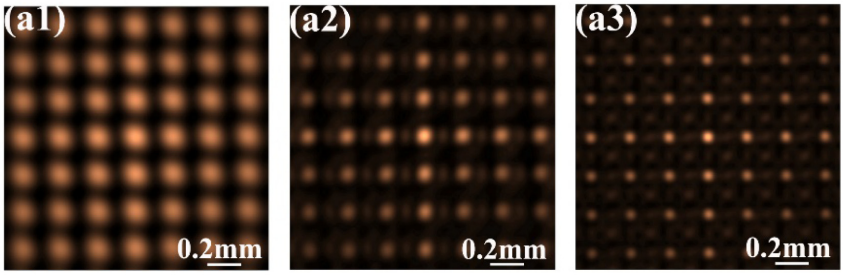

Fig. 7. Experimental results of the squared modulus of the degree of coherence $\left|\mu(x_1, y_1, 1\text{mm}, 1\text{mm})\right|^2$ of the generated radially polarized VOCLs just behind the RPC with $\delta_0 = 0.37\text{mm}$ and $d = 1\text{mm}$ for different values of M and N, (a) $M = N = 2$, (b) $M = N = 3$, (c) $M = N = 5$.

Optics EXPRESS

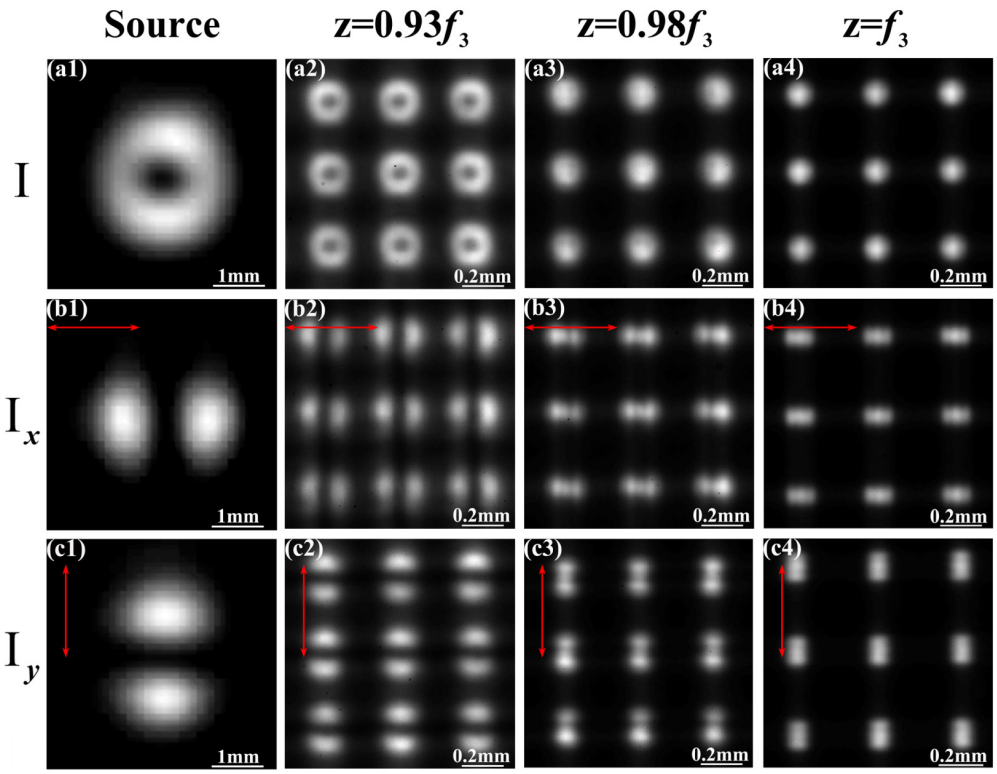

Fig. 8. Experimental results of the intensity distribution of the generated radially polarized VOCLs with $M = N = 3, \delta_0 = 0.37\text{mm}$ and $d = 1\text{mm}$ focused by the thin lens L_3 with focal length $f_3 = 15\text{cm}$ and its corresponding components I_x and I_y at several propagation distances.

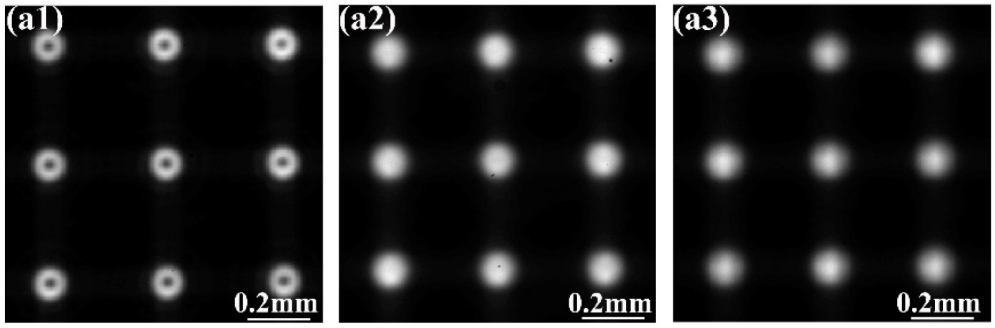

Fig. 9. Experimental results of the intensity distribution of the generated radially polarized VOCLs with $M = N = 3$ and $d = 1\text{mm}$ focused by the thin lens L_3 with focal length $f_3 = 15\text{cm}$ in the focal plane for different values of the coherence parameter, (a) $\delta_0 = 0.6\text{mm}$, (b) $\delta_0 = 0.4\text{mm}$, (c) $\delta_0 = 0.37\text{mm}$.

Figure 7 shows our experimental results for the squared modulus of the radially polarized VOCLs degree of coherence $\left|\mu(x_1, y_1, 1\text{mm}, 1\text{mm})\right|^2$ just behind the RPC with δ_0=0.37mm and $d = 1\text{mm}$ for different values of *M* and *N*. One finds that the exhibited degree of coherence of manifests a lattice-like behavior and the lattice structure becomes progressively more

Optics EXPRESS

complex as magnitudes of M and N increase. Figure 8 shows our experimental results for the intensity distribution and corresponding components I_x and I_y of the generated radially polarized VOCLs with $M = N = 3, \delta_0 = 0.37\text{mm}$ and $d = 1\text{mm}$ focused by the lens L_3 with $f_3 = 15\text{cm}$ at several propagation distances. Figure 9 shows our experimental results for the VOCLs intensity distribution with $M = N = 3$ and $d = 1\text{mm}$ in the focal plane for different values of the coherence parameter δ_0. One infers from Figs. 8 and 9 that a single source beam evolves into an intensity lattice in the focal plane (or the far field), and one can obtain lattices with bright or dark nodes by varying the source coherence parameter. Furthermore, each bright or dark node of the lattice features radial polarization as expected. Our experimental results are consistent with our theoretical predictions.

5. Summary

We have introduced vector optical coherence lattices as a natural extension of recently introduced scalar OCLs, and we have explored the propagation properties of radially polarized VOCLs as a numerical example. In contrast with the scalar OCLs, which generate intensity lattices with bright nodes in the far zone of the source, the radially polarized VOCLs can generate intensity lattices with bright or dark nodes depending on the magnitude of the source coherence parameter. In addition, we have reported the experimental generation of radially polarized VOCLs and characterized their focusing properties. Our experimental results verify our theoretical predictions. Engineering spatial coherence properties of vector beams paves a way for manipulating their propagation properties and for beam shaping. These tools can be useful for trapping multiple particles whose refractive indices are larger or smaller than that of their surroundings, for simultaneous multiple atom trapping and for free-space optical communications.

Funding

National Natural Science Fund for Distinguished Young Scholar (11525418); National Natural Science Foundation of China (11474213, 11374222, 11274005); Project of the Priority Academic Program Development (PAPD) of Jiangsu Higher Education Institutions; National Science and Engineering Research Council of Canada (NSERC).